

Accepted Manuscript

Experimental and Theoretical Analysis of the Elastic-plastic Normal Repeated Impacts of a Sphere on a Beam

Hui Wang , Xiaochun Yin , Xiaoli Qi , Qingming Deng , Bo Yu ,
Qiming Hao

PII: S0020-7683(17)30016-1
DOI: [10.1016/j.ijsolstr.2017.01.014](https://doi.org/10.1016/j.ijsolstr.2017.01.014)
Reference: SAS 9430



To appear in: *International Journal of Solids and Structures*

Received date: 18 September 2016
Revised date: 5 December 2016
Accepted date: 10 January 2017

Please cite this article as: Hui Wang , Xiaochun Yin , Xiaoli Qi , Qingming Deng , Bo Yu ,
Qiming Hao , Experimental and Theoretical Analysis of the Elastic-plastic Normal Repeated Im-
pacts of a Sphere on a Beam , *International Journal of Solids and Structures* (2017), doi:
[10.1016/j.ijsolstr.2017.01.014](https://doi.org/10.1016/j.ijsolstr.2017.01.014)

This is a PDF file of an unedited manuscript that has been accepted for publication. As a service to our customers we are providing this early version of the manuscript. The manuscript will undergo copyediting, typesetting, and review of the resulting proof before it is published in its final form. Please note that during the production process errors may be discovered which could affect the content, and all legal disclaimers that apply to the journal pertain.

Experimental and Theoretical Analysis of the Elastic-plastic Normal Repeated Impacts of a Sphere on a Beam

Hui Wang¹, Xiaochun Yin^{1,*}, Xiaoli Qi², Qingming Deng¹, Bo Yu¹, Qiming Hao¹

¹Department of Mechanics and Engineering Science, Nanjing University of Science and Technology, Nanjing, 210094, China

²School of Mechanics Engineering, Anhui University of Technology, Ma'anshan, 243002, China

*Corresponding author, Email address: yinxiaochun2000@aliyun.com; Fax:+86-25-8431 5875; Tel: +86-25-84315590

Abstract:

The normal repeated impact of a sphere upon an elastic-plastic beam has been analyzed experimentally and theoretically. Hertz elastic contact model and seven well known elastic-plastic contact models were selected for theoretical analysis. A piecewise linearized method has been presented to linearize the nonlinear contact stiffness of eight selected contact models. Generalized closed-form solutions (theoretical solutions) of repeated impact response were derived for each piecewise linearization by vibration theory. Ahead of the theoretical study, to gain a deep insight into the eight selected contact models, an idealized repeated impact problem of elastic-plastic half space/foundation was solved by Runge-Kutta integration method. The numerical results show that the models are of large differences in predicting contact behavior, and reveal a strong correlation of the models with the two model parameters: the indentation of initial contact yield and the effective radius of contact curvature of unloading. Experiments were performed with regard to a repeated impact process of a sphere striking repeatedly at the center of the beam. The theoretical and experimental results show that selecting the appropriate contact model is very

important on predicting contact behavior. No significant advantage of indentation type has been found over flattening type among these contact models. The divergences of contact behavior and the strong correlation for the eight contact models still exist. Compared with the experimental results, for the coefficient of restitution and the rebound velocity of the sphere, all of the eight contact models predict larger values and contrary trends on impact velocity compared to the experimental results. The reasons may come from wave effects and sub-impact phenomenon.

Keywords: Beam, Repeated impact, Experiment, Theoretical solution, Elastic-plastic contact model, Impact response

1 Introduction

The study of elastic-plastic impact behaviors has been at the forefront of engineering research for over a century. Because the plastic deformation behavior within the contact, complicates the relationship between contact force and indentation, the theoretical contact models [1-16] with simplified assumptions have to be presented to reduce greatly the cost of the complicated calculations by numerical methods. When the penetration velocity is smaller than the smallest speed of sound of the impact bodies, the elastic-plastic contact due to impact is considered as quasi-static. Like Hertz elastic contact model [3], the theoretical contact models are also based on the assumption of “half-space”. The elastic-plastic contact deformation and contact stress are assumed to be highly concentrated close to the contact region whose dimensions are relatively small compared to the size of contact bodies. As categorized by Jackson and Kogut [17], most of the theoretical contact models for axi-symmetric contact of solids of revolution are presented for either the flattening or indentation types. For slow velocity impact, the contact region is relatively small, and both the flattening and indentation types are equivalent in half-space contact theory

[3]. Recently, Ghaednia et al. [4] suggested an elastic-plastic contact model for the case of both contact surfaces deforming elastoplastically. Despite of what the models mentioned previously, many other researchers developed numerous analytical elastic-plastic contact models, seen reviews by Ma and Liu [5], Ghaednia et al. [18-19], Machado et al. [20] and Alves et al. [21]. Yet these elastic-plastic contact models only succeeded in characterizing the force-indentation relation for limited materials, geometries, and loading processes, as stated by Ma and Liu [5].

Machado et al. [20] theoretically compared the similarities and differences among the considered dissipative contact models as a result of the dynamic simulations of multi-rigid-body systems. Alves et al. [21] implemented a comparative study of the dissipative contact models with the experiments done by Zhang et al. [22] on the impact between a steel ball and a short cylindrical specimen placed on an iron bulk. Ghaednia et al. [18] examined theoretically and experimentally nine different flattening and indentation contact models to simulate the elastic-plastic oblique impact of a rigid-rod on a flat. The investigations showed that selecting the appropriate contact model is very important. To our knowledge, there is a lack of the theoretically and experimentally comparative study of elastic-plastic contact models on impact problem of elastic-plastic beam. The comparative studies of contact models mentioned previously are limited to single impact problems. However, in machinery, repeated operations can result in repeated impacts [23-25] that usually take place at the same position, and repeated impacts can accumulate plastic deformation [24-25] at this position.

When the beam deflections are small, the indentation law and the pressure distribution in the contact zone are considered to be the same as those of a sphere impacting against a half-space. The elastic-plastic contact models can be applied to

this impact problem of a sphere against a beam [10, 26-30]. Analysis of elastic-plastic beam impact should take into account the interaction between the sphere and the beam, the motion of the sphere and the dynamic response of the beam. The dynamic response of the beam may contain the elastic-plastic contact deformation of the beam, vibration of the beam and wave propagation along the beam. A complete analysis can be done through a three-dimensional finite element model. However, the complex phenomenon of an impact event, especially the interaction between the sphere and the beam, increase the efforts required for simulations. Therefore, different theoretical methods have been used to simplify the problem. The first method simplifies the problem by a two degree-of-freedom spring-mass model by considering the fundamental mode of the beam vibration [28], while the second method simplifies the problem using the truncation of the modal expansion [31]. Both of the two methods model the interaction between the sphere and the beam as a non-linear spring to describe the contact behavior and do not consider the wave propagation. The numerical integration method, such as Runge-Kutta integration method can be applied to obtain a numerical solution. However, the solution is mostly conditionally stable and requires many iteration steps for convergence of the solution. In 2013, Christoforou et al. [10] linearized the contact model presented by Majeed et al. [9], and demonstrated the informative results of the linearized contact model. In 2014, Big-Alabo et al. [32] presented the force-indentation linearization method to investigate the elastic-plastic half-space impact.

The purpose of this study is to investigate theoretically and experimentally the applicability of different contact models on normal repeated impacts of a sphere to an elastic-plastic beam. Hertz elastic contact model and seven well-known elastic-plastic

contact models are selected for theoretical and numerical analysis, and a piecewise linearized method should be developed for theoretical analysis.

2 Contact force formulations

In this section, Hertz model and seven different elastic-plastic contact models are selected. Thornton model [12] is taken as flattening type. Stronge model [6], ML model [5], MYC model [9], CYM model [10] and UC model [33] are taken as indentation type. For convenience, we will classify MJG model [4] as indentation type as the material properties used in the paper are closer to the indentation type.

2.1 Hertz elastic contact model

Goldsmith [26] presented the description of the transverse impact of a sphere on a beam using Hertz theory in detail. Most of the elastic-plastic contact models are using Hertz theory [3] for the elastic loading phase and the unloading phase. Hertz theory uses the equivalent modulus of elasticity and radius:

$$\frac{1}{E^*} = \frac{1-\mu_1^2}{E_1} + \frac{1-\mu_2^2}{E_2}, \frac{1}{R^*} = \frac{1}{R_1} + \frac{1}{R_2} \quad (1)$$

where E_i , R_i , and μ_i are the elastic moduli, the radii and Poisson's ratios of the sphere and the beam, respectively. $R^* = R_1$ for our case since $R_2 = \infty$, if the beam bending curvature is neglected. The elastic contact force, F , is expressed by E^* , R^* , and the indentation δ as follows:

$$F = \frac{4E^* R^{*0.5} \delta^{1.5}}{3} \quad (2)$$

2.2 The division of loading phase

The loading phase has been divided into different sub-phases by different models, as listed in Table 1. In this paper, δ_y is the indentation, in which yield starts, and δ_p is the indentation at onset of the fully plastic phase. Most of the models apply

Johnson's definition of initial contact yield [2] while defining different transition conditions as listed in Table 1. For ML model [6], the onset of the fully plastic phase is governed by two dimensionless parameters: ψ and ε . The parameter ψ takes a fixed value 2.8. The value of ε in the present study is obtained to be 23 by using linear interpolation, according to the data provided by Ma and Liu [5] and the yield stress ratio of the sphere to the beam.

2.3 Two parameters of the unloading phase

The unloading phase starts after the maximum load F_m with the maximum indentation δ_m . As listed in Table 1, except for CYM, MYC and UC models, the force-indentation relation approximately approaches the Hertzian solution:

$$F = \frac{4}{3} E^* (R^{*e})^{0.5} (\delta - \delta_r)^{1.5} \quad (3)$$

where δ_r is the permanent indentation and R^{*e} is the effective radius of contact curvature. The fundamental principle to obtain δ_r and R^{*e} is to keep the continuity of contact force at the transition from loading phase to unloading phase.

By the detailed checking, the solutions of R^{*e} and δ_r suggested by Stronge model [6], can not keep the continuity of contact force. Here, we revise them by assuming that the initial contact force of the unloading phase is equal to the maximum contact force of the loading phase F_m , which is

$$F_m = \frac{4}{3} E^* \sqrt{R^{*e}} (\delta_m - \delta_r)^{1.5} \quad (4)$$

Stronge [6] has presented the geometrical similarity

$$\frac{\delta_y}{R^*} = \frac{(\delta_m - \delta_r)}{R^{*e}} \quad (5)$$

by submitting equation (5) into equation (4), we can obtain revised R^{*e} and δ_r :

$$R^{*e} = \sqrt{\frac{3F_m(R^*/\delta_y)^{1.5}}{4E^*}}, \quad \delta_r = \delta_m - \frac{\delta_y R^{*e}}{R^*} \quad (6)$$

2.4 The reloading phase

For multiple impacts, the loading phase of the second and following impacts is called reloading phase where the previously permanent deformed contact area of the beam remains, but accounts for no residual stress. The reloading phase should be divided into two sub-phases. The first sub-phase follows the unloading phase of the previous impact [10]. The second sub-phase will follow the new loading phase. For models that do not mention the reloading phase, we assume they have the same reloading process as CYM model according to the simulation results of Yan and Li [23].

Stronge and ML models need a threshold values about the permanent indentation, δ_{rp} , defined to indentify the exact phase of the previous loading, respectively. They are solved using Mathematica from equations (7) and (8) respectively:

$$F_y(2\delta_p/\delta_y - 1) \left\{ 1 + (3\delta_y)^{-1} \ln(2\delta_p/\delta_y - 1) \right\} = \frac{4}{3} E^* \sqrt{R^{*e}} (\delta_p - \delta_{rp})^{3/2} \quad (7)$$

$$\delta_p \left(c_1 + c_2 \ln(\delta_p/\delta_y) \right) + c_3 = \frac{4}{3} E^* (R^{*e})^{\frac{1}{2}} (\delta_p - \delta_{rp})^{\frac{3}{2}} \quad (8)$$

where $\delta_p = 84\delta_y$ for Stronge model, and $\delta_p = \varepsilon^2\delta_y/2$ for ML model. F_y is the contact force of initial contact yield, and expressions of c_1, c_2, c_3 can be found in Table 1. If $\delta_r \leq \delta_{rp}$, the previous loading phase belongs to the elastic-plastic phase. If $\delta_r > \delta_{rp}$, the previous contact belongs to the fully plastic phase.

1

Table 1 The formulas of seven different elastic-plastic contact models

Models	Elastic phase	Indentation at yield	Elastic-plastic phase	Unloading phase
UC [33]	$F = \frac{\pi E R \delta^2}{h}$	$\delta_y = \frac{\sigma_y}{E} h$	$F = \pi R \sigma_y (2\delta - \delta_y)$	$F = \pi R E (\delta^2 - \delta_r^2) / h$ $\delta_r = \delta_m - \delta_y$
MYC [9]	$F = \frac{4}{3} E^* R^{0.5} \delta^{1.5}$	$\delta_y = \frac{0.68 \pi^2 \sigma_y^2 R^*}{E^{*2}}$	$F = K_p (\delta - \delta_p) + K_h \delta_p^{1.5}$ $K_h = 4 E^* R^{*0.5} / 3$ $K_p = 1.5 K_h \delta_p^{0.5}$ $\delta_p = 9 \pi^2 k^2 \sigma_y^2 R^* / 16 / E^{*2}$ $k = 1.95$	$F = F_m ((\delta - \delta_r) / (\delta_m - \delta_r))^{1.5}$ $\delta_r = \delta_m - \delta_y (2\delta_m / \delta_y - 1)^{0.5}$
CYM [10]		$\delta_y = \frac{0.68 \pi^2 \sigma_y^2 R^*}{E^{*2}}$	$F = 2 \pi R p_0 \delta$ $p_0 = 2.8 \sigma_y$	$F = F_m (\delta - \delta_r) / (\delta_m - \delta_r)$ $\delta_r = \delta_m - \delta_y (2\delta_m / \delta_y - 1)^{0.5}$
MIJG [4]	$F = \frac{4}{3} E^* R^{0.5} \delta^{1.5}$	$\delta_y = (\frac{\pi C_j \sigma_y}{2 E^*})^2 R^*$ $C_j = 1.295 e^{0.736 \nu}$	$F = F_c [\frac{4 H_G}{C_j \sigma_y} (1 - e^{-\frac{1}{78} \delta^{*5.9}}) \delta^{*1.1} + e^{-0.17 \delta^{*5.12}} \delta^{*1.5}]$ $\delta^* = \frac{\delta}{\delta_y}, \frac{H_G}{\sigma_y} = 2.84 - 0.92 [1 - \cos(\pi a / R)]$ $a = \sqrt{R^* \delta / (1.9 \delta_y)}^B$ $F_c = \frac{4}{3} (\frac{R^*}{E^*})^2 (\frac{\pi C_j \sigma_y}{2})^3$ $B = 0.14 e^{23 \sigma_y / E^*}$	$F = 4 E^* \sqrt{R^*} (\delta - \delta_r)^{3/2} / 3$ $R^* = (3 F_m / 4 / E^*)^2 / (\delta_m - \delta_r)^3$ $\delta_r = \delta_m (0.8 [1 - ((\delta_m / \delta_y + 5.5) / 6.5)^{-2}])$

Continued Table 1

Models	Elastic phase	Indentation at yield	Elastic-plastic phase	Fully plastic phase	Unloading phase
Stronge [6]	$F = \frac{4}{3} E^* R^{*0.5} \delta^{1.5}$	$\delta_y = \left(\frac{3\pi g_y \sigma_y}{4E^*} \right)^2 R^*$ $g_y = 1.1$	$F = F_y \left(\frac{2\delta}{\delta_y} - 1 \right) \left\{ 1 + \frac{\ln(2\delta / \delta_y - 1)}{3g_y} \right\}$ $F_y = \frac{4}{3} E^* R^{*0.5} \delta_y^{1.5}$	$F = 2.8 F_y (2\delta / \delta_y - 1) / g_y$	$F = \frac{4}{3} E^* \sqrt{R^{*e}} (\delta - \delta_r)^{3/2}$ $R^{*e} = \sqrt{\frac{3F_m}{4E^*}} \left(\frac{R^*}{\delta_y} \right)^{1.5}$ $\delta_r = \delta_m - \delta_y R^{*e} / R^*$ $F = \frac{4}{3} E^* \sqrt{R^{*e}} (\delta - \delta_r)^{3/2}$
ML [5]	$F = \frac{4}{3} E^* R^{*0.5} \delta^{1.5}$	$\delta_y = \frac{\pi^2 R^*}{4E^{*2}} p_y^2$ $p_y = 1.6\sigma_y$	$F = \delta (c_1 + c_2 \ln(\delta / \delta_y)) + c_3$ $c_1 = \frac{(2\psi\sigma_y - p_y)\pi R^*}{\ln(\varepsilon^2 / 2)}$ $c_2 = \frac{p_y(1 + \ln(\varepsilon^2 / 2)) - 2\psi\sigma_y}{\ln(\varepsilon^2 / 2)} \pi R^*$ $c_3 = 4E^* R^{*0.5} \delta_y^{1.5} / 3 - c_1 \delta_y$	$F = F_p + k_1(\delta - \delta_p)$ $\delta_p = \varepsilon^2 \delta_y / 2$ $k_1 = c_1 + c_2(1 + \ln(\varepsilon^2 / 2))$ $F_p = \delta_p (c_1 + c_2 \ln(\varepsilon^2 / 2)) + c_3$	$\delta_r = \delta_m - \left(\frac{3F_m}{4E^* \sqrt{R^{*e}}} \right)^{2/3}$ $R^{*e} = \frac{4E^* R^{*1.5} \delta_m^{1.5}}{3F_m} \quad (\delta_m < \delta_p)$ $R^{*e} = \frac{4E^* R^{*1.5} \delta_p^{1.5}}{3F_p} \quad (\delta_m \geq \delta_p)$
Thornton [12]	$F = \frac{4}{3} E^* R^{*0.5} \delta^{1.5}$	$\delta_y = \left(\frac{\sigma_y \pi}{2E} \right)^2 R^*$		$F = F_y + \pi\sigma_y R^* (\delta - \delta_y)$ $F_y = \frac{4}{3} E^* (R^*)^{0.5} \delta_y^{1.5}$	$F = \frac{4}{3} E^* \sqrt{R^{*e}} (\delta - \delta_r)^{3/2}$ $R^{*e} = \frac{4E^*}{3F_m} \left(\frac{2F_m + F_y}{2\pi\sigma_y} \right)^{3/2}$ $\delta_r = \delta_m - \left(\frac{3F_m}{4E^* \sqrt{R^{*e}}} \right)^{2/3}$

3 Simulation results

In this section, an idealized elastic-plastic foundation impact, i.e. an elastic sphere impacting repeatedly on an elastic-perfectly plastic foundation resting on a rigid base, is investigated by UC model. An idealized elastic-plastic half-space impact, i.e. an elastic sphere impacting repeatedly on an elastic-perfectly plastic half space, is studied by the other seven contact models. The deformation is characterized by local indentation of the half-space/foundation, and the vibrations of the half-space/foundation and sphere are negligible. The repeated impact response can be modeled simply by a single degree-of-freedom motion as shown in equation (9). The analysis of idealized elastic-plastic half-space/foundation impact is very useful for validating the contact models, and is meaningful to find the difference and correlation of the contact models.

3.1 Numerical integration solutions

For the theoretical dynamics of the sphere, the differential equation of the motion is:

$$m_1 \mathbf{a}_C = \mathbf{F} - m_1 \mathbf{g} \quad (9)$$

where m_1 is the mass of the sphere, \mathbf{a}_C is the acceleration of the center of the sphere, C , and \mathbf{F} is the total normal contact force. The expressions of the normal contact force are usually nonlinear. Therefore, the equations of motion have been solved numerically using a Runge-Kutta integration method.

The radius of the sphere R_1 is 35mm. The mass of the sphere is 1.40 kg. For UC model, the depth of the elastic-perfectly plastic foundation is $h = 27.8$ mm. The Young's modulus and the yield stress of the elastic-perfectly plastic half-space and foundation are 206 GPa and 345 MPa, respectively. The half-space and foundation are undeformed before the first impact.

A repeated impact process consisting of five impacts has been simulated by using the selected eight contact models. The initial velocity of the sphere for the first impact is $v_0=2.5$ m/s. After the first impact, each of the subsequent impacts allows the sphere strikes the foundation or the half space at the same position with the same initial velocity v_0 , where the contact area has deformed due to the previous impacts.

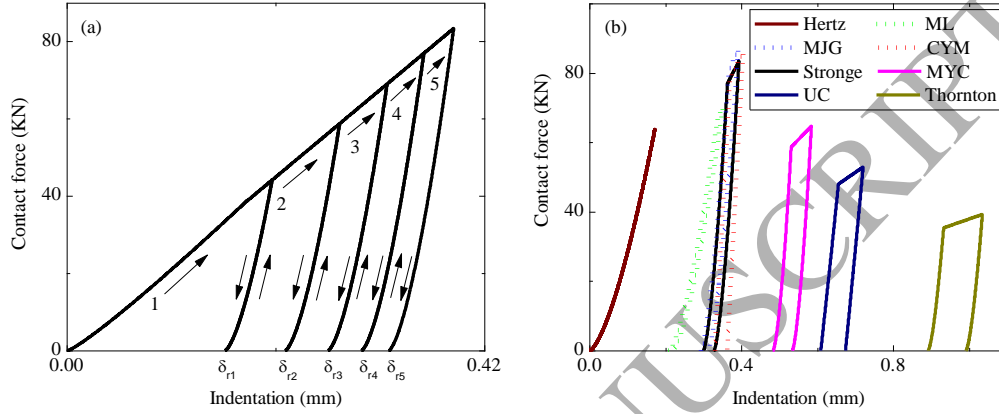


Fig. 1 Force-indentation relationship: (a) 5 impacts of Stronge model, $v_0=2.5$ m/s; (b) the fifth repeated impact of 8 different contact models, $v_0=2.5$ m/s.

In each impact, there is a complete contact cycle including a loading/reloading phase and an unloading phase. Fig. 1(a) shows all the impact processes for Stronge model. The number 1 refers to the first impact with undeformed area. After the first impact, a permanent indentation δ_{r1} remains.

3.2 Differences of the contact models

The most important task of the contact models is to provide the force-indentation relationship. Fig. 1(b) plots the force-indentation relationship of the fifth impact for the eight contact models. The loading process include the elastic loading phase following the unloading phase of the fourth impact and the elastic-plastic loading phase after the previous maximum indentation. It can be seen that, there exist large differences between the different contact models.

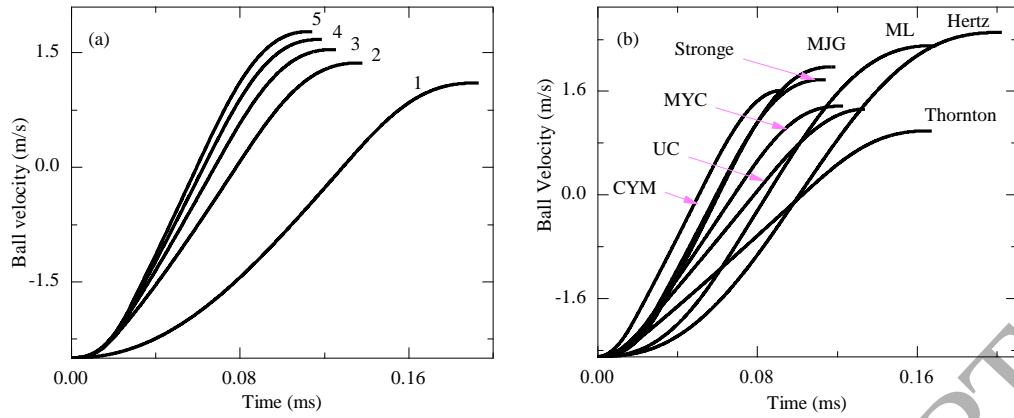


Fig. 2 Velocity-time histories: (a) 5 impacts of Stronge model, $v_0=2.5$ m/s; (b) the fifth repeated impact of 8 different contact models, $v_0=2.5$ m/s.

Fig. 2(a) shows the velocity-time histories of the sphere for five repeated impacts for Stronge model. The velocity of the sphere at the end of every impact (rebound velocity) increases with the number of impacts, but its increment decreases with the number of impacts. Similar variation of the rebound velocity with the number of impacts has been found by Seifried et al. [24] for the repeated impacts performed between a sphere and a rod, where the coefficient of restitution was found to increase until a stationary value was reached with the increase number of repeated impacts. Fig. 2(b) plots the velocity-time histories of the sphere for the fifth repeated impact for the eight contact models. Large differences between the different contact models are found.

As mentioned above, it is found that the contact models are of large differences in predicting contact behavior of repeated impacts, even for the idealized elastic-plastic half-space/foundation impact. The reason is necessary to be investigated for the application of the contact models.

3.3 Definition and theoretical solutions of two equivalent contact stiffnesses

To investigate the large differences between the models in predicting repeated impact response, two equivalent contact stiffnesses, K_{eq} and K_{ueq} should be

defined during loading and unloading phases, respectively.

If the initial velocity of the sphere for the i -th impact is v_{0i} , the impact energy of the sphere is $E_{fi} = \frac{1}{2} m_1 v_{0i}^2$. During the i -th impact, δ_{mi} can be solved theoretically by equation (10) without considering the motion equation of the sphere,

$$E_{U(i-1)} + \int_{\delta_{m(i-1)}}^{\delta_{mi}} F_L(\delta) d\delta = E_{fi}, \quad E_{U(i-1)} = \int_{\delta_{r(i-1)}}^{\delta_{m(i-1)}} F_U(\delta) d\delta \quad (10)$$

where $E_{U(i-1)}$ is the elastic energy released during the previous unloading phase, and $F_L(\delta)$ and $F_U(\delta)$ represent the contact force curve during the loading and unloading phase, respectively, as listed in Table 1. From a given δ_{mi} , the maximum contact force and the permanent indentation δ_{ri} can be solved using the formulas listed in Table 1. The contact stiffnesses K_{eqi} and K_{ueqi} can be expressed theoretically as

$$K_{eqi} = 2(E_{fi} - E_{U(i-1)}) / (\delta_{mi} - \delta_{m(i-1)})^2, \quad K_{ueqi} = 2E_{Ui} / (\delta_{mi} - \delta_{ri})^2 \quad (11)$$

where E_{Ui} is the released elastic energy during the unloading phase.

It is worth noting that the integral equation (10) is a general expression for all of the selected contact models to obtain δ_m . According to equation (10) the analytical expressions of δ_m for all of the selected contact models except for MJG model can be obtained prior to equation (11) by using Mathematica rather than numerical integration. Therefore, we can obtain analytical expressions of K_{eqi} and K_{ueqi} for all of the selected contact models except for MJG model.

There is a simple correspondence between $K_{eq}(K_{ueq})$ and loading/unloading curve in theory. Larger $K_{eq}(K_{ueq})$ is corresponding to stiffer loading/unloading

phase, and then the contact model can be called stiffer contact model. Smaller $K_{eq}(K_{ueq})$ is corresponding to softer loading/unloading phase, and then the contact model can be called softer contact model.

3.4 Correlations of the contact models

Fig. 3 and Fig. 4 show the plots of K_{eq} versus δ_y and the plot of K_{ueq} versus $(R^{*e})^{1/2}$ for the fifth impact, where $v_0=2.5$ m/s. The eight contact models are of large differences in K_{eq} and K_{ueq} . The value of K_{eq} varies from 46.56 to 260.72 MN/m. The value of K_{ueq} varies from 0.30 to 2.05 GN/m. As shown in Fig. 3, for K_{eq} versus δ_y , a strong linear correction is found for the five models: Stronge, ML, CYM, MYC and MJG models. As shown in Fig. 4, for K_{ueq} versus $(R^{*e})^{1/2}$, a strong linear correction is found for all the selected models except for CYM model.

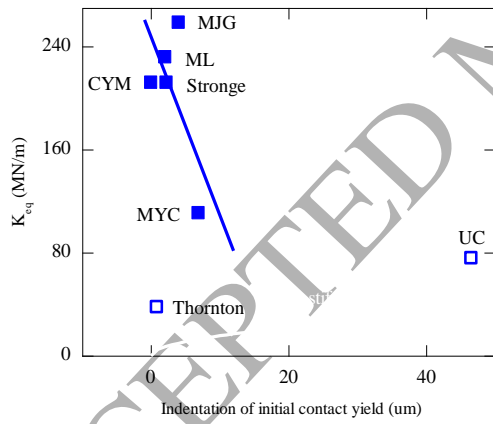


Fig. 3 K_{eq} versus the indentations of initial contact yield

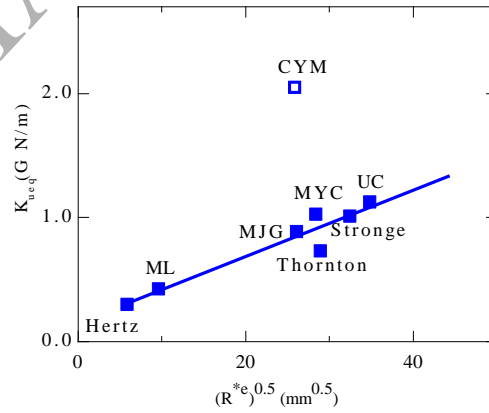


Fig. 4 K_{ueq} versus $\sqrt{R^{*e}}$

Fig. 5 and Fig. 6 show the plots of the contact time versus $K_{eq}^{-2/5} + K_{ueq}^{-2/5}$ and the plot of the rebound velocity versus $K_{eq}^{5/12}(R^{*e})^{-1/6}$ for the fifth impact, where $v_0=2.5$ m/s. The eight contact models are of large differences in the contact time and the rebound velocity. The contact time varies from 91.9 to 202.5 μ s. The rebound

velocity varies from 0.985 to 2.5 m/s. As shown in Fig. 5 and Fig. 6 for all the selected models, two strong linear corrections are found either for the contact time versus $K_{eq}^{-2/5} + K_{ueq}^{-2/5}$ or for the rebound velocity versus $K_{eq}^{5/12} (R^*e)^{-1/6}$.

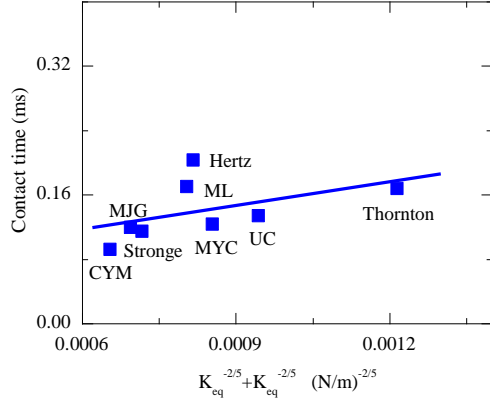


Fig. 5 Contact time versus $K_{eq}^{-2/5} + K_{ueq}^{-2/5}$

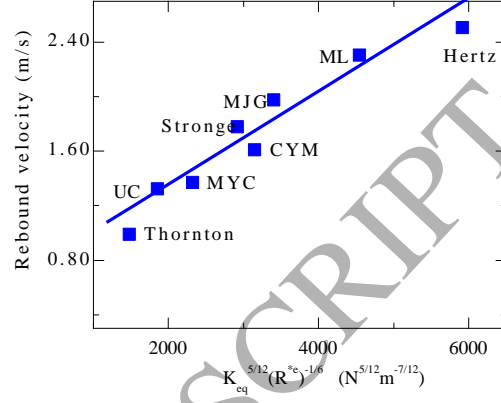


Fig. 6 Rebound velocity of the sphere versus $K_{eq}^{5/12} (R^*e)^{-1/6}$

Fig. 7 shows the plots of $(\delta_m - \delta_r)$ versus $K_{eq}^{5/12} (R^*e)^{-1/6}$ for the fifth impact, where $v_0=2.5$ m/s. The eight contact models are of large differences in $(\delta_m - \delta_r)$. The value of $(\delta_m - \delta_r)$ varies from 41.90 to 172.07 μm . For all the selected models, a strong linear corrections is found for $(\delta_m - \delta_r)$ versus $K_{eq}^{5/12} (R^*e)^{-1/6}$.

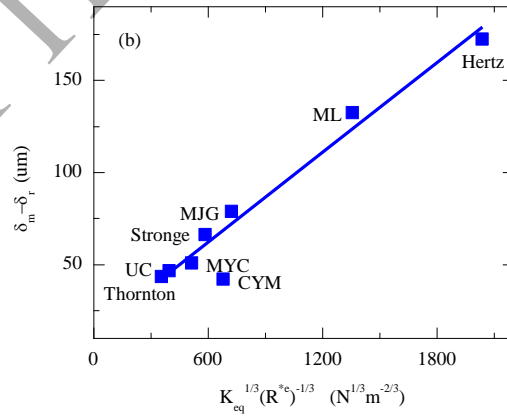


Fig. 7 $\delta_m - \delta_r$ versus $K_{eq}^{1/3} (R^*e)^{-1/3}$

From the correlation studies mentioned above, the selected contact models independently presented by the previous researchers have strong correlation. The

strong positive/negative linear correlations are found between the key values of repeated impact response and the carefully selected correlation parameters. The selected correlation parameters are combined by K_{eq} , K_{ueq} and R^{*e} that are originally from indentation of initial contact yield and R^{*e} . It is concluded that large differences in predicting repeated impact response are originally resulted from the divergences of indentation of initial contact yield and R^{*e} selected by the contact models.

4 Theoretical solution

In the previous section, the repeated impact response of the idealized elastic-plastic half-space/foundation has been investigated by means of numerical integration solutions. In this section, a nominal case of study is selected to investigate the application of the contact models on flexible structures. It corresponds to a repeated impact problem of elastic-plastic beam, i.e. a steel sphere striking repeatedly on a simply supported steel beam.

As shown in Fig. 1, both the first and fifth impacts behave as piecewise linear behavior of contact force-indentation approximately. It is instructive to present a piecewise linearized method for the piecewise linearization of contact force-indentation relationship during repeated impacts.

4.1 Two degrees of freedom spring-mass model

Fig. 8 shows a two degree-of-freedom spring-damper-mass model, where x_1 is the displacement of the sphere, x_2 is the displacement of the contact point of the beam, and the indentation of the sphere δ is $(x_1 - x_2)$. The local elastic-plastic contact deformation is modeled as a spring with piecewise linearized contact stiffness k_1 . The beam motion is modeled as a spring-mass model with the static stiffness k_2 and the equivalent mass m_2 . The energy dissipation by damping is modeled as damper with a

constant coefficient of viscous damping c . The motion of the sphere is modeled as rigid mass m_1 without damping, and the elasticity of the sphere is involved in local contact deformation by the contact models. The static stiffness k_2 can be calculated from the beam static stiffness of impact point, and $m_2 = k_2 / \omega_2^2$, can be calculated by considering the fundamental natural frequency ω_2 and the static stiffness k_2 .

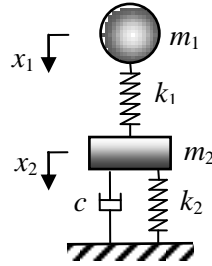


Fig. 8 Two degree-of-freedom spring-damper-mass model

4.2 Piecewise linearized method

For an originally selected contact model, the linearization of its nonlinear contact force-indentation relationship will be realized with the aid of the definition of K_{eq} and K_{ueq} in section 3. The contact model after linearization is called as linearized contact model. Its force-indentation relationship can be expressed in a uniform form,

$$F = k_1 \delta + f_s, \quad \delta = x_1 - x_2. \quad (12)$$

where F is the linearized contact force. For a selected contact model, in each impact phase, k_1 is different. In each impact, k_1 and the coefficient f_s are different for loading/reloading and unloading phases. If repeated impacts take place and the permanent contact deformation of the beam remains, the reloading phase should be divided into two sub-phases. The first sub-phase follows the unloading phase of the previous impact. The second sub-phase will follow the new loading phase.

For the i -th impact ($i > 1$), during the first sub-phase of the reloading phase,

$$k_1 = F_{m(i-1)} / (\delta_{m(i-1)} - \delta_{r(i-1)}), \quad f_s = -k_1 \delta_{r(i-1)} \quad (13)$$

For the i -th impact ($i \geq 1$), during the second sub-phase of the reloading phase,

$$f_s = -k_1 \delta_{m(i-1)} + F_{m(i-1)} \quad (14)$$

$$k_1 = 2(\delta_{mi} - \delta_{m(i-1)})^{-2} \int_{\delta_{m(i-1)}}^{\delta_{mi}} F_L(\delta) d\delta \quad (15)$$

For the i -th impact ($i \geq 1$), during the unloading phase,

$$k_1 = F_{mi} / (\delta_{mi} - \delta_{ri}), \quad f_s = -k_1 \delta_{ri} \quad (16)$$

where δ_{ri} is calculated by the expression of the original contact model listed in Table

1. The expressions of δ_{mi} and $\int_{\delta_{m(i-1)}}^{\delta_{mi}} F_L(\delta) d\delta$ can be derived analytically from equation (10) for all of the selected contact models, except for MJG model. To consider the beam deformation, equation (15) can become an iterative algorithm to update δ_{mi} by generalized closed-form solutions of repeated impact response that will be presented in section 4.3.

4.3 Generalized closed-form solutions

For each phase of loading/reloading and unloading of the repeated impact problem of elastic-plastic beam, the vibration equation (17) of the two degree-of-freedom system shown in Fig. 8 can be solved by the vibration theory. Generalized closed-form solutions are expressed in the form of equation (18):

$$\mathbf{M}\ddot{\mathbf{x}}(t) + \mathbf{C}\dot{\mathbf{x}}(t) + \mathbf{K}\mathbf{x}(t) = \mathbf{f} \quad (17)$$

$$\mathbf{u}(t) = \mathbf{U}(t)\mathbf{u}_0 + \mathbf{V}(t)\dot{\mathbf{u}}_0 + \int_0^t \mathbf{h}(t-\tau)\mathbf{f}d\tau \quad (18)$$

where t is time variable, and \mathbf{M} , \mathbf{K} , \mathbf{C} and \mathbf{f} are the mass matrix, stiffness matrix, damping matrix and excitation matrix, respectively,

$$\mathbf{M} = \begin{bmatrix} m_1 & 0 \\ 0 & m_2 \end{bmatrix}, \quad \mathbf{K} = \begin{bmatrix} k_1 & -k_1 \\ -k_1 & k_1 + k_2 \end{bmatrix}, \quad \mathbf{C} = \begin{bmatrix} 0 & 0 \\ 0 & c \end{bmatrix}, \quad \mathbf{f} = \begin{bmatrix} m_1 g - f_s \\ f_s \end{bmatrix}. \quad (19)$$

\mathbf{u}_0 and $\dot{\mathbf{u}}_0$ are the initial displacement and velocity vectors, respectively. $\mathbf{U}(t)$,

$\mathbf{V}(t)$ and $\mathbf{h}(t)$ are expressed as [34]:

$$\mathbf{U}(t) = \Phi \text{diag}[U_r(t)] \Phi^{-1}, \quad \mathbf{V}(t) = \Phi \text{diag}[V_r(t)] \Phi^{-1}, \quad \mathbf{h}(t) = \mathbf{V}(t) \mathbf{M}^{-1} \quad (20)$$

$1 \leq r \leq 2$ $1 \leq r \leq 2$

where Φ is the eigenvector matrix. $U_r(t)$ and $V_r(t)$ are expressed as:

$$U_r(t) = e^{-\zeta_r \bar{\omega}_r t} \left(\cos \sqrt{1 - \zeta_r^2} \bar{\omega}_r t + \frac{\zeta_r}{\sqrt{1 - \zeta_r^2}} \sin \sqrt{1 - \zeta_r^2} \bar{\omega}_r t \right) \quad (21)$$

$$V_r(t) = \frac{e^{-\zeta_r \bar{\omega}_r t}}{\omega_r \sqrt{1 - \zeta_r^2}} \sin \sqrt{1 - \zeta_r^2} \bar{\omega}_r t \quad (22)$$

where $\bar{\omega}_r$ ($r=1, 2$) is the natural frequency, and ζ_r is:

$$\zeta_r = \frac{C_r}{2\sqrt{M_r K_r}} \quad (23)$$

The generalized mass matrix M_r , generalized stiffness matrix K_r , and generalized damping matrix C_r can be expressed respectively as:

$$M_r = \Phi_r^T \mathbf{M} \Phi_r, \quad K_r = \Phi_r^T \mathbf{K} \Phi_r, \quad C_r = \Phi_r^T \mathbf{C} \Phi_r \quad (r=1, 2) \quad (24)$$

For the repeated impact problem of elastic-plastic beam, we consider a repeated impact process consisting of N impacts. The impact velocity of the sphere of the i -th impact is v_{0i} . In every impact, the beam stays initially at rest. There is no permanent deformation of the beam for the first impact, but the accumulated permanent deformation of the beam remains for subsequent impacts. For the application of the generalized closed-form solutions, the time variable and the initial condition need to be adjusted.

4.4 Verifications

Stronge model is applied to verify the linearized contact model for a repeated

impact process including five impacts. The initial impact velocity of the sphere is 2.5m/s in every impact. A $780 \times 60 \times 27.8$ mm steel simply supported beam is impacted at the centre of span by a 35 mm radius steel ball. The masses of the sphere and the beam are $m_1=1.40$ kg and $M_2=10.15$ kg, respectively. The material of the beam is considered to be elastic-perfectly plastic with Young's modulus of 206 GPa and yield stress of 345 MPa. Young's modulus and yield stress of the sphere are 206 GPa and 580 MPa, respectively. The static stiffness of the simply supported beam $k_2=2238256$ N/m. The fundamental natural frequency of the beam ω_2 is 667.90 rad/s. The equivalent mass of the simply supported beam is $m_2=5.00$ kg. The damping coefficient c , $c=298$ kg/s, is obtained from the experimental data to consider damping. The test method will be explained in detail in section 5.4. The linearized contact model is obtained by the piecewise linearized method from Stronge model. It predicts the repeated impact response theoretically by the generalized closed-form solutions. Stronge model simulates the repeated impact response numerically by solving the nonlinear vibration equation using a Runge-Kutta integration method.

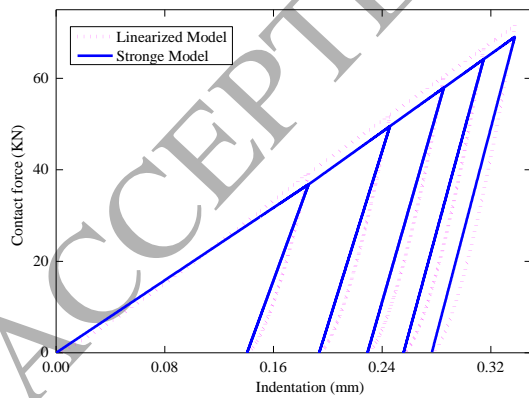


Fig. 9 Force-indentation relationship during repeated impact process

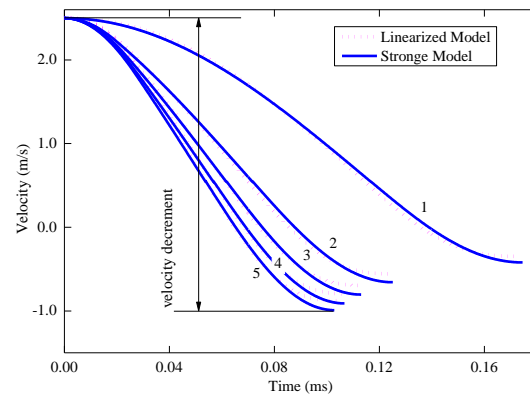


Fig. 10 Velocity-time histories of the sphere

Fig. 9 shows a complete contact force-indentation relationship of the five impacts. During any one of impacts, the linearized contact model predicts the

maximum contact force a little below than that simulated by Stronge model. The error of the maximum contact force is less than 5.4%. The two contact models predict the same values on the accumulated permanent indentations. The linearized contact model can ensure the continuity of contact force and indentation at the transition point from the loading phase to unloading phase. In addition, for the first impact, only three iterative steps are needed to produce convergent solution and for the subsequent impacts, two iterative steps are needed.

Fig. 10 shows the velocity-time histories of the sphere for the five impacts. For any one of impacts, the error of the rebound velocity predicted by the linearized contact model is less than 19.3%. However, the velocity of the sphere predicted theoretically by the linearized contact model is well agreement with that simulated by Stronge model during loading/reloading phase and the first half phase of unloading. For any one of impacts, the error of velocity decrement of the sphere calculated by the linearized contact model is less than 3.4%. The above comparison results show that the linearized contact model can predict repeated impact responses reasonably well.

5 Experiments

5.1 Experimental setup

The experimental setup, shown in Fig. 11, originally developed by Qi et al. [35], has been built for the normal impact of a sphere upon a beam. In this paper, the experimental setup is used to measure repeated impact response of a steel sphere striking repeatedly upon a steel beam. A dropping device has been designed to provide variable initial impact velocities for the experiments. A laser displacement sensor is used to measure the normal displacement of the beam under the impact point. The measurement circuit is designed to measure the contact time, where the circuit is opened when the impact starts and closed when the impact ends. The accumulated

permanent indentation is measured after every impact. The data acquisition equipment with the collection frequency of 100 KHz has been used to record the experimental data.

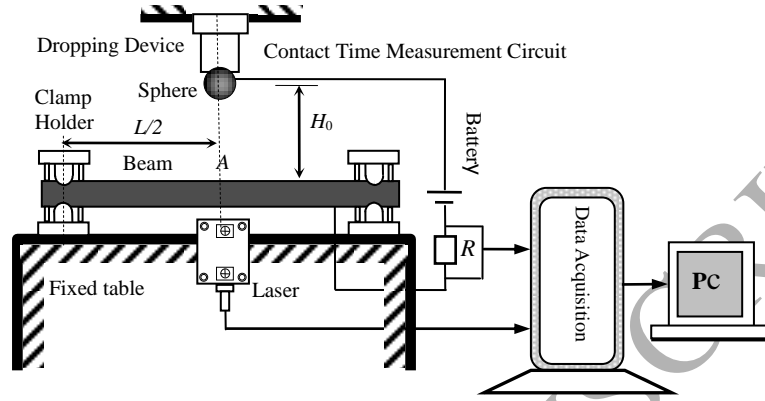


Fig. 11 Sketch of the experimental setup, front view

5.2 Material property and geometry

The material properties and the geometry of the sphere and the beam are listed in Table 2. Particularly, we consider the beam material to be elastic-perfectly plastic according to our uniaxial tension test, see Fig. 12.

Table 2 The material properties of the sphere and the simply supported beam

Sphere (Gr 15)		Simply supported beam (Q345)	
R_1	0.035 (m)	L	0.780 (m)
		h	0.0278 (m)
		b	0.0600 (m)
ρ_1	7800 (kg/m ³)	ρ_2	7800 (kg/m ³)
m_1	1.400 (kg)	M_2	10.15 (kg)
E_1	208 (GPa)	E_2	210 (GPa)
σ_{y1}	580 (MPa)	σ_{y2}	345 (MPa)
ν_1	0.3	ν_2	0.3

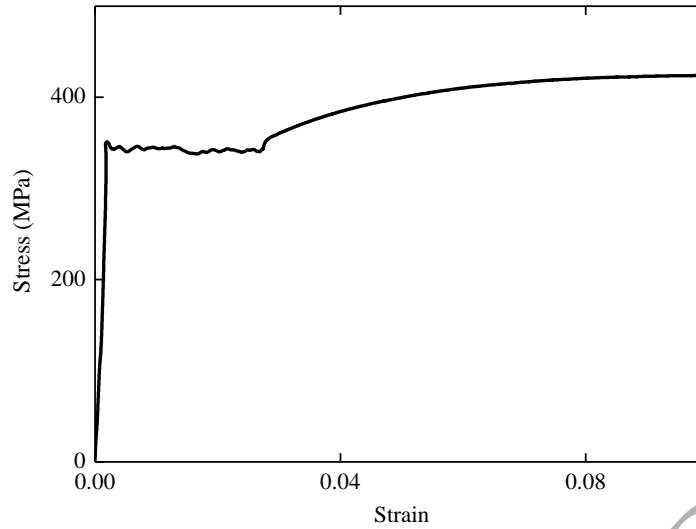


Fig. 12 Uniaxial tension test of the beam material

5.3 Design of repeated impact process

The experiments are performed at position A (the center of the beam), which has been marked in Fig. 11. A complicate repeated impact process consisting of 91 impacts is designed for comprehensive investigation of repeated impact behavior. Table 3 lists the release height and the number of impacts at this release height. In this paper, the experimental response of the last impact of every release height is chosen for comparison with theoretical solutions.

Table 3 The release height and the number of impacts

Height (mm)	Number of impacts	Height (mm)	Number of impacts	Height (mm)	Number of impacts	Height (mm)	Number of impacts
50	4	130	7	210	3	290	3
60	3	140	2	220	8	300	2
70	3	150	2	230	2	310	1
80	3	160	2	240	5	320	1
90	3	170	2	250	2	330	3
100	2	180	4	260	2	340	3
110	2	190	2	270	2	350	1
120	2	200	7	280	2	360	1

5.4 Parameter determinations

The first-order vibration frequency of the experimental beam is obtained by using the Fourier spectrum analysis of measured signal of the beam displacement. It is

106.48 Hz, which is well agreement with the theoretical first-order vibration frequency 106.30 Hz, so that the experimental beam can be assumed to be a simply supported beam. Hence, the static stiffness of the experimental beam $k_2 = 2238256$ N/m. Because the fundamental natural frequency of the experimental beam ω_2 is 669.03 rad/s, the equivalent mass of the simply supported beam is $m_2 = 5.00$ kg.

The damping coefficient c can be obtained by natural logarithm processing of the peak data of the experimental beam displacement [34]. Here the experimental data of the third impact of release height 70 mm is used. To involve the wave impedance, u_1 and u_2 are selected during the initial stage of impact response. The damping coefficient is calculated to be 298 kg/s. This damping coefficient may also include the structural damping.

5.5 Calculation of coefficient of restitution

The coefficient of restitution (COR) is defined as the ratio of relative velocity between post-impact and pre-impact [36-37]. In the experiments, the sub-impact phenomenon has been observed at every release height of the sphere. By ignoring motion damping of the sphere, the rebound velocity of the sphere at the end of the first sub-impact is obtained from the sphere's equations of motion:

$$v_{rebound} = \frac{g(t_i - t_b)^2 - 2u_b(t_b) + 2u_b(t_i)}{2(t_i - t_b)} \quad (25)$$

where t_b and t_i are the end time of the first sub-impact and the beginning time of next sub-impact, respectively, measured by the measurement circuit; $u_b(t_b)$ and $u_b(t_i)$ are the measured displacements by the laser displacement sensor of the point on the back of the beam that is corresponding to the contact point. The velocity of the beam contact point is obtained by taking the derivative of the beam displacement with

respect to time. In the experiments, the relative rebound velocity is calculated by the velocity of the sphere minus the velocity of the beam contact point.

6 Results and comparisons

For the theoretical solutions, a two degree-of-freedom linear spring-mass model is applied as shown in Fig. 8, where $m_1=1.40$ kg, $k_2=2238256$ N/m, $m_2=5.00$ kg, and $c=298$ kg/s. The nonlinear contact stiffness of an original contact model is piecewise linearized by the piecewise linearized method presented in section 4.2. Applying the generalized closed-form solutions presented in section 4.3, the theoretical solutions can be obtained for the repeated impact response of the experimental impact system. In this section, for every release height of the sphere, the response of the last impact is chosen for comparison between experiments and theoretical solutions.

As has been found by Pashah et. al. [28], several impacts may exist before the sphere definitely separates from the beam. We call these impacts as sub-impacts. The sub-impacts will complicate the impact behavior [28,35,38-39]. In this paper, we focus merely on the first sub-impact if the phenomenon of sub-impacts occurs. In general, the first sub-impact maintains the contact state about 0.1~1 ms, and our experiment results show that the contact time is about a few hundred microseconds.

6.1 Comparison of contact time

Fig. 13 shows the contact time as a function of impact velocity of the sphere. All of the models show similar trend. The contact time decreases with the increase of impact velocity of the sphere. For smaller impact velocity of the sphere, Hertz model matches the experimental results well, while other models predict smaller contact time than the experimental results. For larger impact velocity of the sphere, ML model predicts slightly smaller contact time than the experimental results. Hertz model

predicts larger contact time and other models predict smaller contact time than the experimental data. Thornton, Stronge, MYC, MJG, CYM and UC models show some fluctuation of the contact time. Such a fluctuation is observed in the experiments, and may be due to the complicated repeated impact process.

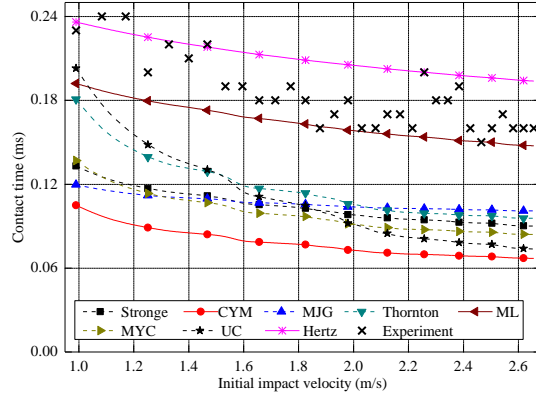


Fig. 13 Contact time of the theoretical solutions and experiments

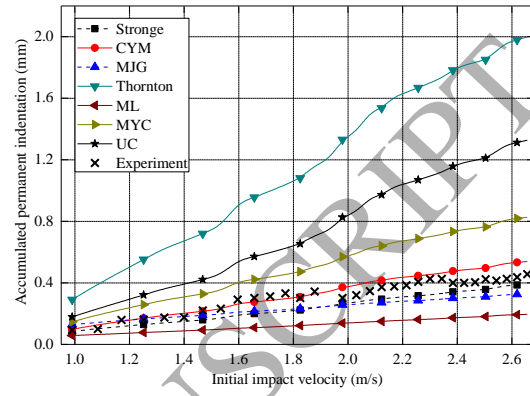


Fig. 14 Accumulated permanent indentation of the theoretical solutions and experiments

As the same as that shown in Fig. 5, Fig. 13 also shows that Hertz model predicts the largest result, ML model predicts the result a little smaller than Hertz model and CYM model predicts the smallest result. The model sequence shown in Fig. 13 in order of the predicting value of contact time is almost the same as that shown in Fig. 5. It concludes that the correlations of the contact models will not be affected largely by the global structural deformation and complicated repeated impact process.

6.2 Comparison of permanent indentation

Fig. 14 shows the accumulated permanent indentation δ_r as a function of impact velocity of the sphere. All of the models show similar trend. The accumulated permanent indentation δ_r increases almost linearly. Thornton, MYC and UC models predict the largest values, while ML model predicts the smallest values. Stronge and MJG models behave closely. Stronge, CYM and MJG models predict the accumulated permanent indentation well matched with the experimental results for smaller impact

velocity, while MJG and Stronge models match the experimental data well for larger impact velocity. Thornton, Stronge, MYC, MJG and CYM models show some fluctuation. Such a fluctuation is observed in the experiments, and may be due to the complicated repeated impact process. The comparison between the theoretical solutions and the experiments illustrates that δ_r predicted by soft models (MYC, UC and Thornton models) is too large, but stiff models (CYM, MJG and Stronge models) can predict δ_r in better agreement with the experimental data. It concludes that the correlations of the contact models will not be affected largely by the global structural deformation and complicated repeated impact process.

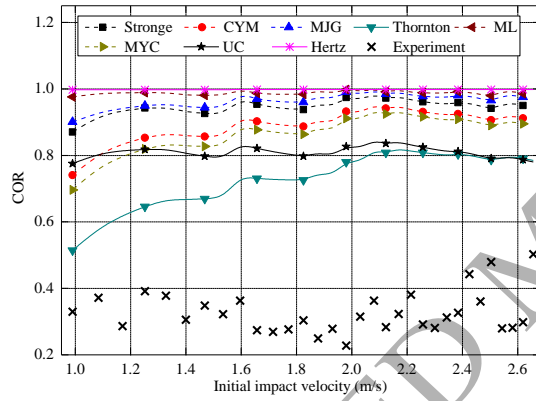


Fig. 15 Coefficient of restitution of the theoretical solutions and experiments

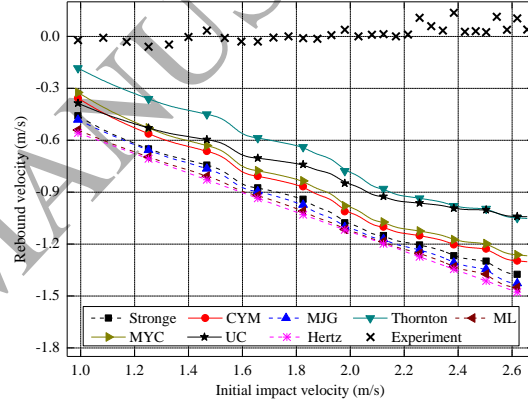


Fig. 16 Rebound velocity of the sphere of the theoretical solutions and experiments

6.3 Comparison of coefficient of restitution

Fig. 15 shows the coefficient of restitution (COR) as a function of impact velocity of the sphere. All the models other than Hertz model show similar trend. Hertz model is elastic, and the corresponding coefficient of restitution is unity. COR predicted by ML model approaches unity. As the impact velocity of the sphere increases, COR predicted by Stronge and MJG models also approaches a constant slightly smaller than unity. Thornton model predicts the smallest COR. Among the elastic-plastic contact models, ML model predicts the largest COR. As the impact

velocity of the sphere increases, COR predicted by Thornton and UC models approach to a same value. Overall, none of the models matches the experimental results well. All of the models predict much larger COR than the experimental data. The fluctuation can also be found in the experimental and theoretical results which might be due to the complicatedly repeated impacts.

6.4 Comparison of rebound velocity

As shown in Fig. 15, it has been found that all the selected models predicted too larger COR than the experimental data. To investigate the reason, Fig. 16 shows the rebound velocity of the sphere as a function of impact velocity of the sphere. All of the models show similar trend. The absolute rebound velocity increases with increasing impact velocity of the sphere. The experimental rebound velocity increases slightly with increasing impact velocity of the sphere. However, most of the experimental results are positive while the prediction results of the models are always negative.

As the same as that shown in Fig. 6, Fig. 16 also shows that Hertz model predicts the largest rebound velocity, ML model predicts the rebound velocity a little smaller than Hertz model, and Thornton model predicts the smallest rebound velocity. The model sequence shown in Fig. 16 in order of the predicting value of rebound velocity is almost the same as that shown in Fig. 6. It concludes that the correlations of the contact models will not be affected largely by the global structural deformation and complicated repeated impact process.

Fig. 16 illustrates that the absolute value of rebound velocity has large difference between the models and experiments. This might be due to the effect of sub-impacts on the theoretical solutions. In the experiment, sub-impact phenomenon has been found for every impact test. When the rebound velocity of the sphere is positive as

shown in Fig. 16 for the experiment, the sphere moves in the same direction with the beam after the first sub-impact, and then subsequent sub-impacts can occur. The subsequent sub-impacts will increase the rebound velocity of the sphere. But the theoretical solutions for all the models predict negative rebound velocity, and the sub-impacts could not be simulated.

On the other hand, wave effects may be an important influence factor that result in small COR and rebound velocity in experiments. The influence of wave effects on the impact of a beam and a sphere will be investigated for further study.

7 Conclusions

In this study, the dynamics of the normal repeated impact of a sphere upon an elastic-plastic beam has been analyzed experimentally and theoretically. The repeated impact response was modeled as a two degree-of-freedom spring-damper-mass motion for theoretical analysis. A piecewise linearized method has been presented to piecewise linearize the nonlinear contact stiffness of eight selected contact models. Generalized closed-form solutions of impact responses were derived for each piecewise linearization by vibration theory, by which the theoretical solution of the repeated impact response was obtained. The theoretical solution was verified by the numerical integration solution using the original contact models.

Selecting the appropriate contact model is very important and gives different results for either the loading phase or the unloading phase, including the force-indentation curve, the time history of contact force and the time history of sphere velocity. No significant advantage of indentation type has been found over flattening type among these contact models. The contact time, the accumulated permanent indentation, and the coefficient of restitution calculated from the experiments are compared with the theoretical solutions using different contact

models. The experiment provides more impact results for flexible structures, which can be used for checking the validation of a contact model and its predicting accuracy.

The divergences of contact behavior for eight different contact models have been analyzed from simulations. The stiffness of loading is found to be strongly dependent upon the condition of initial contact yield, while the stiffness of unloading strongly depends on calculating method of the effective radius of contact curvature of unloading. The contact time, the rebound velocity of sphere and the accumulated permanent indentation demonstrate strong linear correlations to model parameters, and those model parameters can be traced back to the two parameters, indentation of initial contact yield and effective radius of contact curvature of unloading. The two parameters are crucial in determining the outcome in the contact models. The strong correlation of the contact models has not been influenced significantly by the global elastic deformation of the structure and complicated repeated impact process.

Comparing with the experimental results, it has been shown that for the contact time, Hertz model matches the experimental results well under the circumstances of small impact velocities. For accumulated permanent indentation, Stronge and MJG models are in good agreement with the experimental results. For the coefficient of restitution and the rebound velocity of the sphere, all of the eight contact models predict larger values and contrary trends on impact velocity compared to the experimental results. The reasons may come from wave effects and sub-impact phenomenon.

ACKNOWLEDGEMENTS

The work was supported partially by the National Natural Science Foundation of China (Grant No. 11372138 and No. 11572157), the Research Fund for the Doctoral Program of Higher Education of China (20123219110036) and Industry University

Research Joint Innovation Fund - Prospective Joint Research Project (BY2014004-06), the supports are gratefully acknowledged.

References

- [1] Pal RK, Awasthi AP, Geubelle PH. Wave propagation in elasto-plastic granular systems. *Granular Matter* 2013;15(6): 747-58.
- [2] Johnson KL, Contact mechanics. Cambridge : Cambridge university press; 1987.
- [3] Hertz H. Über die Berührung fester elastischer Körper. *Journal für die reine und angewandte Mathematik* 1882; 92: 156-71.
- [4] Ghaednia H, Marghitu DB, Jackson RL, Predicting the permanent deformation after the impact of a rod with a flat surface, *Journal of tribology* 2014, 137(1): 011403.
- [5] Ma DL, Liu CH. Contact law and coefficient of restitution in elastoplastic spheres. *Journal of Applied Mechanics* 2015; 82(12): 121006.
- [6] Stronge WJ. Impact mechanics. Cambridge : Cambridge University Press; 2000.
- [7] Brake MR. An analytical elastic-perfectly plastic contact model. *International Journal of Solids and Structures* 2012; 49(22): 3129-41.
- [8] Brake MRW. An analytical elastic plastic contact model with strain hardening and frictional effects for normal and oblique impacts. *International Journal of Solids and Structures* 2015; 62: 104-23.
- [9] Majeed MA, Yigit AS, Christoforou AP. Elastoplastic contact/impact of rigidly supported composites. *Composites Part B Engineering* 2012; 43(3): 1244-51.
- [10] Christoforou AP, Yigit AS, Majeed MA. Low-velocity impact response of structures with local plastic deformation: characterization and scaling. *Journal of Computational and Nonlinear Dynamics* 2013; 8(1): 149-56.

- [11] Majeed MA, Yigit AS, Christoforou AP. Modeling and analysis of elastoplastic impacts on supported composites. *Key Engineering Materials* 2011; 471:367-72.
- [12] Thornton C. Coefficient of restitution for collinear collisions of elastic-perfectly plastic spheres. *Journal of Applied Mechanics* 1997; 64(2): 383-6.
- [13] Vu-Quoc L, Zhang X. An elastoplastic contact force–displacement model in the normal direction: displacement–driven version. *Proceedings of the Royal Society of London. Series A* 1999; 455(1991): 4013-44.
- [14] Vu-Quoc L, Zhang X, Lesburg L. A normal force-displacement model for contacting spheres accounting for plastic deformation: force-driven formulation. *Journal of Applied Mechanics* 2000; 67(2): 363-71.
- [15] Kogut L, Etsion I. Elastic-plastic contact analysis of a sphere and a rigid flat. *Journal of Applied Mechanics* 2002; 69(5): 657-62.
- [16] Jackson RL, Green I. A finite element study of elasto-plastic hemispherical contact against a rigid flat. *Journal of Tribology* 2005; 127(2): 343-54.
- [17] Jackson RL, Kogut L. A comparison of flattening and indentation approaches for contact mechanics modeling of single asperity contacts, *Journal of tribology* 2006, 128(1): 209-12.
- [18] Ghaednia H, Cermik O, Marghitu DB. Experimental and theoretical analysis of the elasto-plastic oblique impact of a rod with a flat. *International Journal of Impact Engineering* 2015; 86: 307-17.
- [19] Ghaednia H, Pope SA, Jackson RL, Marghitu DB. A comprehensive study of the elasto-plastic contact of a sphere and a flat. *Tribology International* 2016; 93: 78-90.
- [20] Machado M, Moreira P, Flores P, Lankarani HM. Compliant contact force models in multibody dynamics: Evolution of the Hertz contact theory. *Mechanism*

and Machine Theory 2012; 53(7): 99-121.

[21] Alves J, Peixinho N, Silva MTD, et al. A comparative study of the viscoelastic constitutive models for frictionless contact interfaces in solids. *Mechanism & Machine Theory* 2015; 85: 172–88.

[22] Zhang Y, Sharf I. Validation of nonlinear viscoelastic contact force models for low speed impact. *Journal of Applied Mechanics* 2009; 76(5): 911-4.

[23] Yan S, Li L. Finite element analysis of cyclic indentation of an elastic-perfectly plastic half-space by a rigid sphere. *Proceedings of the Institution of Mechanical Engineers, Part C: Journal of Mechanical Engineering Science* 2003; 217(5): 505-14.

[24] Seifried R, Schiehlen W, Eberhard P. Numerical and experimental evaluation of the coefficient of restitution for repeated impacts. *International Journal of Impact Engineering* 2005; 32(1): 508-24.

[25] Schiehlen W, Seifried R, Eberhard P. Elastoplastic phenomena in multibody impact dynamics. *Computer Methods in Applied Mechanics and Engineering* 2006; 195(50): 6874-90.

[26] Goldsmith W. *Impact: The Theory and Physical Behavior of Colliding Solids*. London: Edward Arnold Publishers; 1960.

[27] Ruan HH, Yu TX. Local deformation models in analyzing beam-on-beam collisions. *International Journal of Mechanical Sciences* 2003; 45(3): 397-423.

[28] Pashah S, Massenzio M, Jacquelin E. Prediction of structural response for low velocity impact. *International Journal of Impact Engineering* 2008; 35(2): 119-32.

[29] Yigit A, Christoforou A. Impact dynamics of composite beams. *Composite Structures* 1995; 32(1): 187-95.

[30] Christoforou AP, Yigit AS. Scaling of low-velocity impact response in composite structures. *Composite Structures* 2009; 91(3): 358-65.

- [31] Pashah S, Massenzio M, Jacquelin E. Structural response of impacted structure described through anti-oscillators. *International Journal of Impact Engineering* 2008; 35(6):471-86.
- [32] Big-Alabo A, Harrison P, Cartmell M P. Algorithm for the solution of elastoplastic half-space impact: Force-indentation linearisation method. *Proceedings of the Institution of Mechanical Engineers, Part C: Journal of Mechanical Engineering Science* 2015; 229(5): 850-8.
- [33] Abrate S. *Impact on Composite Structures*. Cambridge: Cambridge University Press; 1998.
- [34] Hu H Y, *Mechanical vibrator foundation*. Beijing: Beijing university press; 2005.
- [35] Qi XL, Yin XC, Wang W, Yang HB, et al. Design and Numerical Simulation of Experimental System for Multiple Elastic-plastic Impacts. *Journal of Nanjing University of Science and Technology* 2012; 36(2): 202-6.
- [36] Zhang X, Vu-Quoc L, A method to extract the mechanical properties of particles in collision based on a new elasto-plastic normal force-displacement model, *Mechanics of Materials* 2002, 34 (12) :779-94.
- [37] Zhang X, Vu-Quoc L, Modeling the dependence of the coefficient of restitution on the impact velocity in elasto-plastic collisions, *International Journal of Impact Engineering* 2002, 27 (3): 317-41.
- [38] Stoianovici D, Hurmuzlu Y. A critical study of the applicability of rigid-body collision theory. *Journal of Applied Mechanics* 1996; 63(2): 307-16.
- [39] Yin XC, Qin Y, Zou H. Transient responses of repeated impact of a beam against a stop. *International Journal of Solids and Structures* 2007; 44(22): 7323-39.